Journal of AI and Data Mining
Vol 6, No 1, 2018, 35-46

Automatic Optic Disc Center and Boundary Detection in Color Fundus Images

F. Abdali-Mohammadi[1*] and A. Poorshamam [2]

1. Faculty of Engineering, Department of Computer Engineering & Information Technology, Razi University, Kermanshah, Iran.
2. Faculty of Basic Science, Department of Mathematic. Razi University, Kermanshah, Iran.

Received 09 November 2015; Revised 18 June 2016; Accepted 05 March 2017
**Corresponding author: fardin.abdali@razi.ac.ir (F. Abdali-Mohammadi).*

Abstract
Accurate detection of retinal landmarks like the optic disc is an important step in computer-aided diagnosis frameworks. This paper presents an efficient method for the automatic detection of the optic disc center and estimating its boundary. The center and initial diameter of the optic disc are estimated by employing an artificial neural network (ANN) classifier, which employs the visual features of vessels and their background tissue to classify the extracted main vessels of retina into two groups: vessels inside the optic disc and vessels outside optic disc. To this end, the average intensity values and standard deviation of RGB channels, the average width and orientation of the vessels, and density of the detected vessels and their junction points in a window around each central pixel of main vessels are employed. The center of the detected vessels, which belong to the inside of the optic disc region, is adopted as the optic disc center, and their average lengths in the vertical and horizontal directions are selected as the initial diameter of the optic disc circle. Then the exact boundary of the optic disc is extracted using the radial analysis of the initial circle. The performance of the proposed method is measured on the publicly available DRIONS, DRIVE, and DIARETDB1 databases, and compared with several state-of-the-art methods. The proposed method shows a much higher mean overlap (70.6%) in the same range of detection accuracy (97.7%) and center distance (12 pixels). The average sensitivity and predictive values of the proposed optic disc detection method are 80.3% and 84.6%, respectively.

Keywords: *Retinal Image Segmentation, Optic Disc Center Detection, Optic Disc Border Estimation.*

1. Introduction

The eye and retinal diseases such as diabetic retinopathy, occlusion, and glaucoma are the major causes of blindness in the developed and developing countries. The detection and quantitative measurement of different parts of retina such as blood vessels, optic disc, and fovea, is an important step in the computer-aided diagnosis of these diseases. Manual or semi-automatic detection of retinal landmarks is labor-intensive and time-consuming, especially in a large database of retinal images. Thus the development of automatic methods for robust detection of these landmarks is valuable. In the literature, several techniques have been reported for detecting and analyzing retinal landmarks like blood vessels [1-8], fovea [9, 10], and optic disc [11-34].

The optic disc is an important landmark for registering changes within the optic disc region due to a retinal disease. The changes in the shape, color or depth of the optic disc are used to measure abnormal features due to certain retinopathies such as glaucoma and diabetic retinopathies [4, 10-12]. It can also be used for detecting other anatomical components like fovea [14, 15]. This region has different properties, and in the literature, several methods attempt to employ one or more characterizations of it to estimate the location of the optic disc region. The optic disc is usually the brightest component on the fundus images, and therefore, a set of high-intensity pixels can be identified as the optic disc location [16-19]. The application of threshold to intensity values may work well unless there are

other high-intensity components such as exudates and lesion regions.

Another feature that can be used to detect the optic disc is the intensity variation in this region because of dark blood vessels beside the bright nerve fibers [15, 16]. However, this method often fails when a large number of white lesions or light arti-facts exist in the fundus images.

Since the vessels are originated from the center of the optic disc, some methods have tried to find the strongest vessel network convergence as the primary feature for detection of the optic disc. The center of the optic disc can be estimated as the convergence point of vessels [20, 21].

The direction of vessels in the optic disc is another feature of this region that has been used to estimate the location of the optic disc [22, 23]. Since the directions of the main vessels inside the optic disc are vertical, Youssif et al. [22] have proposed the directional matched filter to highlight this feature of the optic disc region. The center of the optic disc is estimated as a point with the highest response to the directional matched filter.

Other techniques such as principal component analysis (PCA) [24], texture descriptor [25], Radon transform [26], and morphological operations [24, 27, 28] have also been used to estimate the location of the optic disc.

Some methods have tried to employ the complex feature vector obtained from the vessel network and background of the optic disc region to classify all pixels of the input image into two groups: optic disc region and non-optic disc region [29-34].

Also the optic disc boundary has been extracted by employing different techniques such as fixed circle [15], active contour models [19], genetic algorithm [18], and watershed transform [21].

In this paper, an efficient method is presented for automatic extraction of the optic disc location and boundary. To this end, the visual characteristics of the optic disc region are employed to distinguish the main vessels inside the optic disc using the artificial neural network (ANN) classifier. The center of detected vessels is adopted as the center of optic disc, and an average length of detected vessels in horizontal and vertical directions is used as the initial diameter of the optic disc circle. The precise location of the optic disc boundary is determined using the radial analysis of this circle.

The rest of this paper is organized as what follows. The proposed method for an efficient optic disc detection is presented in section 2. Experimental results are reported in section 3. Finally, conclusion is given in section 4.

2. Proposed Optic Disc Detection method

In the fundus images, as shown in figure 1, the optic disc is known as a high intensity or yellowish region. It is the entrance point of the blood vessels and optic nerves. The occurrence of the dark blood vessels beside the light optic nerves also causes a relatively rapid variation in the intensity of this region. The thickness of the blood vessels gradually reduces when distant from the optic disc center. The main blood vessels split into smaller branches, and spread out to the whole retinal surface for delivering and receiving blood supplies in the capillary system. Some of these features have been employed in the literature for localization of the optic disc. To perform robust optic disc detection, one should employ all of these features, especially in abnormal cases.

Figure 1. Color fundus image.

This paper presents a supervised method for the automatic detection of the optic disc region. To increase the reliability of detection of the optic disc center and boundary, we limited the search process to the centerline of the detected main vessels in the retinal images. By employing this limitation, not only the white lesion regions can be neglected from the list of optic disc candidates but also the speed of the search process can be increased. At first, the main vessels of retina are detected, and for each vessel point, all characteristics of the vessels and their background tissue are extracted as a feature vector. Then by employing the ANN classifier, all the detected vessel points will be classified into two classes: inside the optic disc (IOD) and outside the optic disc (OOD) vessels. Finally, the center of the IOD vessels is selected as the optic disc center and the average length of the IOD vessels in horizontal and vertical directions is used as the initial diameter of the optic disc circle. Then the precise location of the optic disc boundary is determined using the radial analysis of this circle. The flowchart of the proposed method is shown in figure. 2.

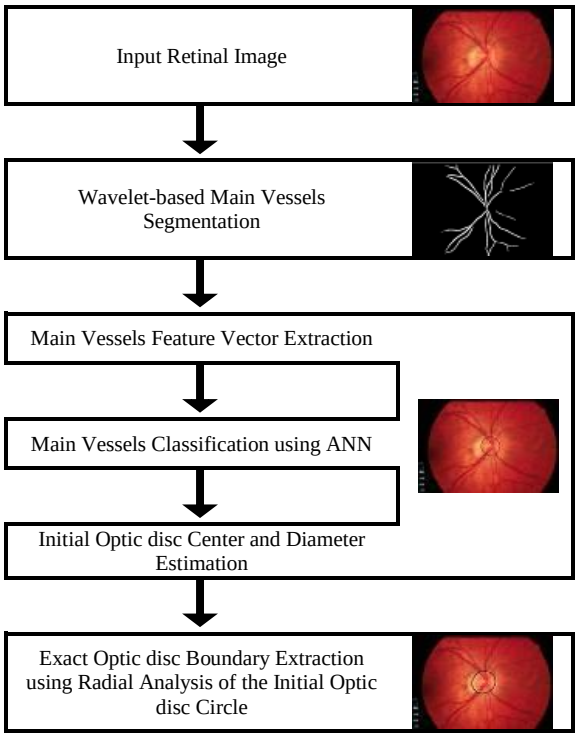

Figure 2. Flowchart of proposed method for automatic detection of center and boundary of optic disc.

2.1. Main vessels segmentation

To extract the main blood vessels, we employed a multi-resolution analyzing technique based on continuous wavelet transform [3]. In this method, complex Morlet was used as the analyzing wavelet to enhance the Gaussian-shaped line structures (vessel structures) and separate them from other non-vessel edges like edges of red lesions and bright blobs. The final vessel network is extracted by applying an adaptive thresholding process. The basic threshold value (TB) was obtained by analyzing the cumulative density function (CDF) obtained from the histogram of the vesselness values (real part of complex Morlet coefficients). Since the average ratio of all the thin and thick vessel pixels in the retinal images is less than 15% [3], and also to detect the optic disc, thick vessels are sufficient, we set the basic threshold value such that its value was equal to 90% of the existing vesselness values:

$$T_B = \arg_j \{\mathrm{CDF(j)} = 0.90\} \qquad (1)$$

The imaginary part of the complex Morlet coefficient in each pixel is added to the basic threshold value in order to penalize the edge-shaped points. After applying an adaptive thresholding procedure, a proper length filter is also applied to the result obtained to eliminate small regions. (For more details, refer to Ref. [3].) An example of the different steps involved in the segmentation phase is shown in figure 3.

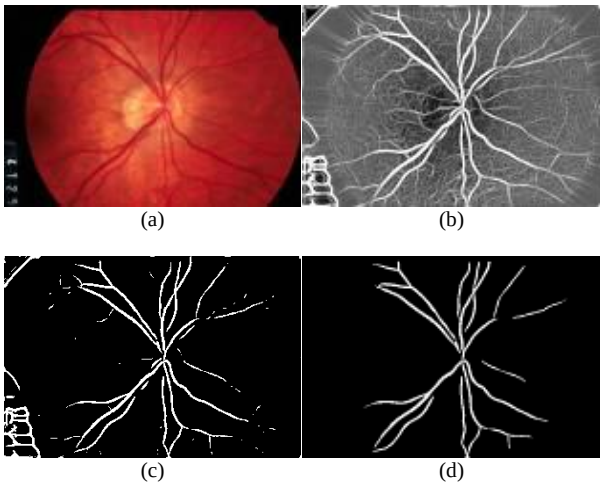

Figure 3. Results obtained in vessel segmentation phase. a) Original fundus image. b) Enhanced vessels using wavelet-based technique. c) Results of applying adaptive thresholding. d) Final detected main vessels.

2.2. Main vessels feature vector extraction

To calculate different features from vessels, we introduced a simplified variation of the local vessel pattern operator [35] and applied it to the center line of the detected main vessels. The simple local vessel pattern (*SLVP*) operator is defined using N equally-spaced points ($P_R(i)$ for i = 0 to $N-1$) on a circle with radius R, which is centered at the centerline pixel (x_c,y_c) of the detected vessels (***I***):

$$P_R(i) = I([x_C - R\sin(2\pi i/N)],[y_C + R\cos(2\pi i/N)]) \qquad (2)$$

The coordinate of each point is rounded ([.]) so that its position exactly falls into the center of a pixel. Therefore, the value of each point $P_R(i)$ is equal to "1" if it falls on the vessel points and "0" otherwise. The number of points (N) in *SLVP* is set to the number of pixels existing in the perimeter of the corresponding circle ($\lceil N = 2\pi R \rceil$). Also the radius of the circle is adopted such that the *SLVP* obtained can describe the certain features of all vessel structures. Since in the retinal images with their size of about 565 × 584 pixels (DRIVE datasets [36]) the maximum width of blood vessels (W_X) is less than 10 pixels, we set the value for radius R to 15 pixels in order to span all vessel widths. For other datasets that have a large difference to this size, this radius should be set based on its maximum width of vessels plus five ($R = W_X + 5$). Another choice is employing the resizing algorithm to resize the images to about 565 × 584 pixels (size of images in the DRIVE dataset).

By analyzing the obtained circular structure of the SLVP operator, different features of vessel points such as vessel width (V_w), vessel orientation (V_θ), and vessel junctions (J_V) can be extracted. The

type of each vessel point can be determined using the number of vessel ends (V_E) that intersect with the perimeter of the corresponding circle. Each vessel end consists of one transition from 0 to 1, several 1s, and one transition from 1 to 0. Therefore, half of the number of transitions from 0 to 1 or vice versa can be used as the number of vessel ends (V_E), as below:

$$V_E = \frac{1}{2}\left(|P_R(N-1) - P_R(0)| + \sum_{i=0}^{N-2} |P_R(i) - P_R(i+1)| \right) \quad (3)$$

Therefore, the type of current point can be determined as one of these cases based on the value of V_E:

- If $V_E \leq 2$, the current point is simple or end vessel point.
- If $V_E > 2$, the current point is a junction (bifurcation or cross-over) point.

Also the width (V_w) and orientation (V_θ) of vessel can be estimated as below:

$$V_w = 2R \times \sin(\frac{\pi N_v}{N})$$
$$V_\theta = \frac{(POFO + N_v/2) \times 2\pi}{N} \bmod \pi \quad (4)$$

where, R is the radius of the circular structure and N is the number of all points in the circular structure. Also *POFO* is the position of the first point with value "1" from the beginning of the obtained circular structure and N_v is the average number of vessel points in the vessel ends. Therefore, the value for N_v should be calculated from the number of all vessel points existing in the circular structure divided by the number of vessel ends:

$$N_v = (\sum_{i=0}^{N-1} P_R(i)) / V_E \quad (5)$$

An example of extracting *SLVP* for $R = 15$ and $N = 96$ (P_{15}) and the details of estimating *POFO* and N_v are also illustrated in figure 4.

To detect the IOD vessels, all visual characteristics of the vessels and their background tissue are employed as a feature vector. To increase the reliability of the measured features, all features are calculated in a 70 × 70 window (W) centered at each point (x, y) in the centerline of the detected main vessels. Then the following set of features is measured:

1) Average intensity value in the window W for red (I_R), green (I_G), and blue (I_B) channels of the colored retinal image (Im):

$$I_C = \sum_{x,y \in W} \mathrm{Im}(x,y,C) / |W| \quad for\ C \in \{R,G,B\} \quad (6)$$

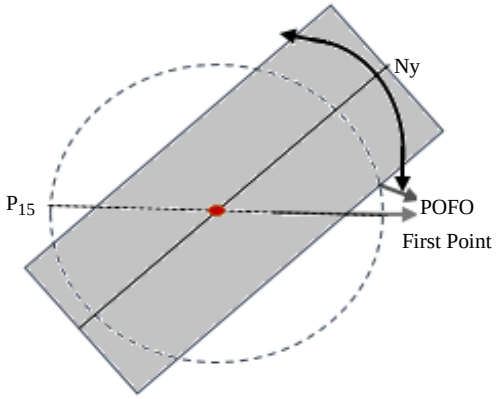

Figure 4. An example of extracting local vessel pattern for *R = 15* and *N = 96* and estimation of *POFO* and N_v. Value of white circle is one (for vessel points) and black circle is zero (for non-vessel points).

where, |W| is the number of points in the window W.

2) Standard deviation of intensity value in the window W for red (S_R), green (S_G) and blue (S_B) channels of colored retinal image (Im):

$$S_C = \sqrt{(\sum_{x,y \in W} (\mathrm{Im}(x,y,C) - I_C)^2) / |W|} \quad for\ C \in \{R,G,B\} \quad (7)$$

3) Average width of the vessels in the window W:

$$A_w = (\sum_{x,y \in W} V_w(x,y)) / |N_V^W|$$

(8)

where, $|N_V^W|$ is the number of vessel centerline points in the window W.

4) Average orientation of the vessels in the window W:

$$A_\theta = (\sum_{x,y \in W} V_\theta(x,y)) / |N_V^W| \quad (9)$$

5) Density of the detected vessels (V) in the window W:

$$D_V = (\sum_{x,y \in W} V(x,y)) / |W| \quad (10)$$

6) Density of junction points (J_V) of vessels in the window W:

$$D_J = (\sum_{x,y \in W} J_V(x,y)) / |N_V^W| \quad (11)$$

2.3. Initial optic disc circle extraction

To increase the reliability of detection of the optic disc center and boundary, we limited the search process to the centerline of the main vessels in the retinal images. To separate the vessels inside the optic disc from the other main vessels, all visual characteristics of the vessels and their background

tissue were extracted as a feature vector ($\vec{F}$) for each centerline point of the main vessels:

$$\vec{F} = \{I_R, I_G, I_B, S_R, S_G, S_B, A_\theta, A_w, D_V, D_J\} \quad (12)$$

Then the extracted feature vectors for all centerline points were applied to a fully connected multi-layer perceptron ANN to be applied to a fully connected multi-layer perceptron to estimate their similarity to the IOD or OOD vessels. This ANN had 10 input neurons, 7 hidden neurons, and one output neuron. The ANN output indicated the similarity of the input feature vector to the IOD vessels (S_{IOD}) and in the range of 0 to 1. The values near 1 were related to the IOD vessels, and those near 0 were related to the OOD vessels. The structure of the proposed ANN is shown in figure 5.

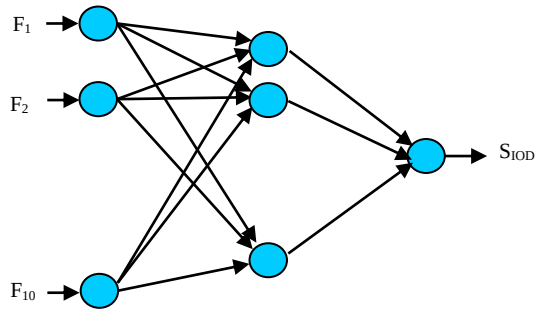

Figure 5. Structure of employed ANN to estimate similarity of main vessel to IOD vessels. Input F_k is k^{th} element of extracted feature vector corresponding to main vessel point, and S_{IOD} is similarity value of this vessel point to inside of optic disc vessels.

After estimating the similarity of all points on the centerline of main vessels to the IOD vessels by the proposed ANN, the points with S_{IOD} values greater than 0.5 were selected as the IOD vessel candidates. Then the morphological closing operator (using disk structure element with radius of 20 pixels) was applied to the IOD candidates to connect the near disjointed candidates. The biggest set of candidates was selected as the IOD vessels.

Finally, the center of detected IOD vessels was selected as the optic disc center, and the average length of IOD vessels in the horizontal and vertical directions was used as the diameter of the initial optic disc circle. The details of these steps are given in figure 6.

2.4. Exact optic disc boundary detection using radial analysis

Since the intensity of the optic disc region is very high, and it can be more visible in the red channel, this channel was selected for further processing (see Figures 7a-7c). At first, the morphological opening operator was applied to the red channel to reduce the effect of dark vessels in the optic disc region. Then the final location of the optic disc boundary was determined using the radial analysis of initial optic disc circle on the enhanced red channel. Therefore, the position of each point on the initial optic disc circle was adjusted to a new point on the radial line whose intensity was near the optic disc boundary intensity.

To this end, for each point on the initial circle perimeter (called "Initial Position"), a radial line was defined as a line that passed through the corresponding point in the direction of the initial circle radius. The length of this line was set to the length of the radius of the initial circle, and the corresponding point fell exactly at the middle of this line (one half at inside the circle and the other half at outside of it). The position of each point on the radial line was rounded to fall on a nearest pixel. On the radial line, at first, the direction of adjustment was determined. Therefore, five points starting from Initial Position toward inside were considered, and we compared their intensities with a pre-defined threshold (the average intensity of optic disc points TOD). If the intensity of all of them was greater than the threshold TOD, the direction of adjustment was set to the outside of the initial circle, and the final position of this point was adjusted to the first point whose value was lower than the threshold TOD. Otherwise (the intensity of all of them not greater than the threshold TOD), the direction of adjustment was set to the inside of the initial circle, and the final position of this point was adjusted to the first point whose value was greater than the threshold TOD. The value for threshold TOD was set to average intensity of pixels inside the initial circle on the enhanced red channel. Finally, the morphological closing operator was applied to the adjusted border to smooth the boundary and fill the small gaps that may exist in the region of vessels. The details of the proposed method are given in figure 7.

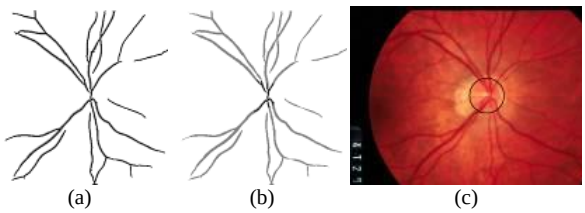

Figure 6. Results of different steps of obtaining initial optic disc circle. a) Extracted main vessel center line. b) Detected IOD vessels. c) Initial optic disc circle.

3. Experimental results

The proposed method for automatic optic disc center detection and its boundary estimation was evaluated on three publicly available databases, the DRIONS database [18], DRIVE database [36], and DIARETDB1 database [37].

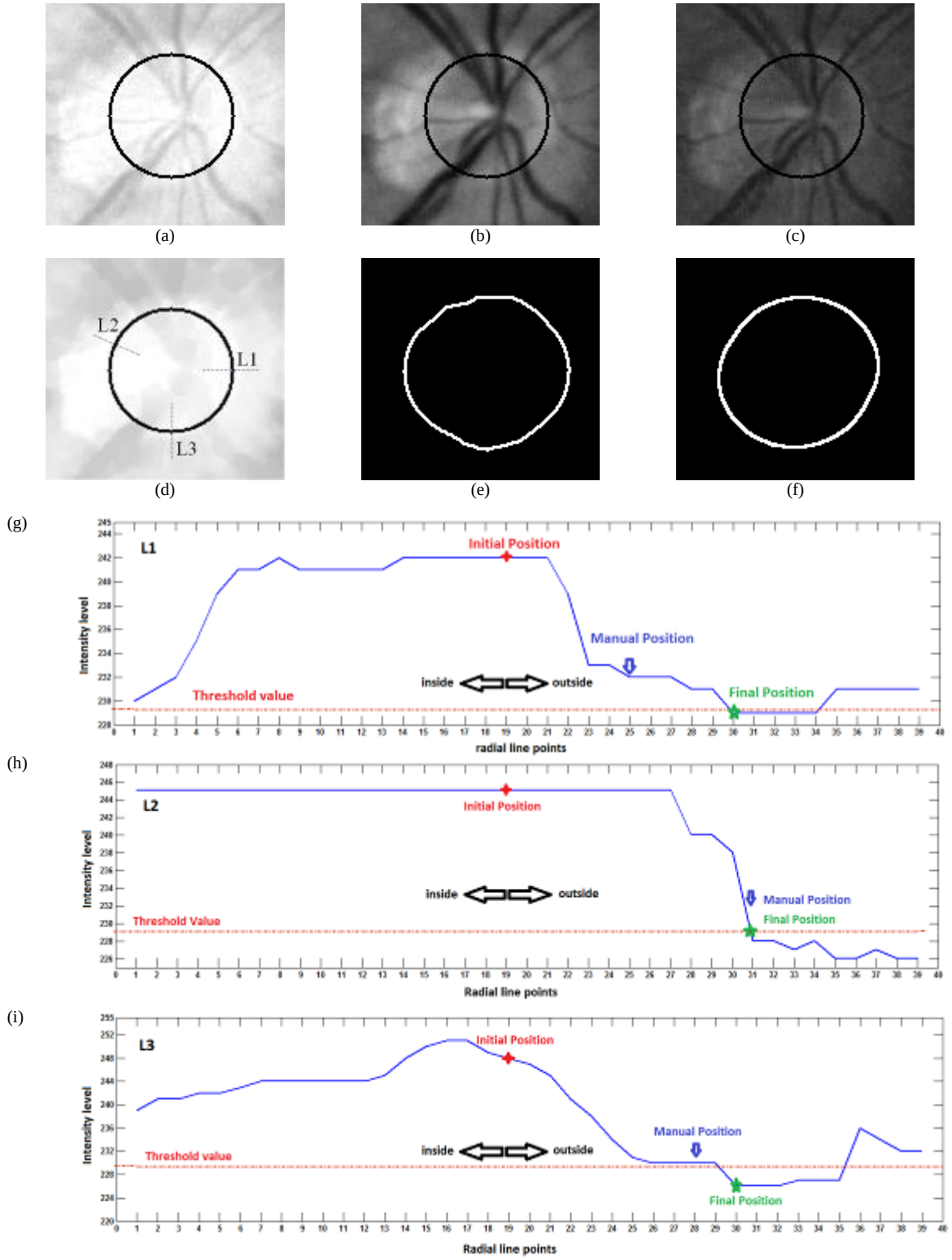

Figure 7. Details of radial analysis for adjusting border of optic disc. a) Initial optic disc circle on red channel (Initial Position). b) Initial optic disc circle on green channel. c) Initial optic disc circle on blue channel. d) Enhanced red channel for applying radial analysis method along with three radial lines L1, L2, and L3.) Finally, adjusted optic disc boundary (Final Position). f) True optic disc boundary extracted by expert (Manual Position). h-i) Details of applying radial analysis method on three radial lines L1, L2, and L3.

The DRIONS dataset consists of 110 images. This set has the same images used in Carmona et al. [18]. These images were captured in digital form using a HP-Photosmart S20 fundus camera at 45° field of view (FOV). The size of images was 600 × 400 pixels, and we used 8 bits per each color channel. Two experts manually segmented the optic disc region of all images. The union of hand-labeled images by two experts was used as ground truth.

The DRIVE database consists of 40 images along with manual segmentation of vessels. It has been divided into training and test sets, each of which containing 20 images. These images were captured in digital form using a Canon CR5 3CCD camera at 45° FOV. The size of images was 565 × 584 pixels, and 8 bits per each color channel were used. We hand-labeled the optic disc regions by one expert, and used them as ground truth.

DIARETDB1 is an image database consisting of 89 color eye fundus images along with manual detected optic disc region. The size of images is 1500 × 1152 pixels. These images were captured using a fundus camera at 50° FOV.

To evaluate the proposed method, based on the area overlap between the ground truth optic disc region and the optic disc region obtained by the proposed method, different parameters such as true positive (TP), false negative (FN), and false positive (FP) were calculated. TP is the area of the ground truth optic disc region also detected by the proposed method. FN is the area of the ground truth optic disc region that was not detected by the proposed method. FP is the area of the detected optic disc region that is outside the ground truth optic disc region, as shown in figure 8.

Using these metrics, we can obtain more meaningful performance measures like sensitivity, predictive, and overlap values, as below:

$$\text{Sensitivity} = TP / (TP + FN) \quad (13)$$

$$\text{Predictive} = TP / (TP + FP) \quad (14)$$

$$\text{Overlap} = TP / (TP + FP + FN) \quad (15)$$

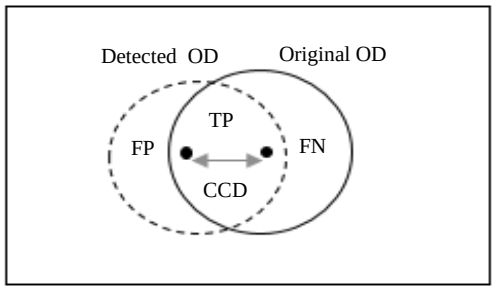

Figure 8. Areas used to estimate performance of proposed method. CDD is Euclidian distance between detected center and original center of optic disc.

Also to evaluate the performance of the optic disc detection algorithm, accuracy (ACC) and center disk distance (CDD) from the original position was used as measure. ACC is defined as the percentage of the images that the detected optic disc has overlapped with the ground truth images. CDD is also defined as the Euclidean distance between the center of the detected optic disc and the center of reference optic disc in the ground truth images.

At First, to obtain the best structure for ANN, we divided the images for the DRIONS dataset into two equal sets (each with 55 images): one set was used as the training set and the other one as the test set. We trained ANN with different numbers of nodes in the hidden layer. The training was done using the gradient decent algorithm and repeated 100 epochs for each input. This process was done when the number of hidden nodes in ANN were set to 2, 3, 4, 5, 6, 7, 8, 9, 10, 15, and 20 neurons. In each case, the performance of ANN was evaluated using the test images. The results obtained are shown in table 1. From the results obtained, the best performance was related to the case where the number of hidden nodes was set to 7 neurons. Therefore, we used this ANN in the remaining experiments.

To evaluate the proposed method on all images of the DRIONS dataset, the test and train sets were exchanged, and the performance of the proposed method was calculated again. The average of the obtained performances along with the results of Carmona et al. [18] are summarized in table 2.

Table 1. Results obtained for proposed method for different numbers of hidden neurons in ANN.

Hidden Nodes	2	3	4	5	6	7	8	9	10	15	20
ACC%	96.3	96.3	98.1	98.1	100	100	100	100	98.1	98.1	96.3
Overlap%	70.4	72.2	73.4	76.5	77.6	77.7	77.2	76.8	75.4	74.9	72.3
CDD (pixel)	14.4	13.8	12.2	11.8	10.9	8.8	10.3	11.2	12.8	13.4	13.7

From the results obtained, ACC, CDD, and overlap of the proposed method were 100%, 9 Pixels, and 76.5%, respectively. Some samples of the results obtained for the proposed method are shown in figure 9. To compare the proposed method with some of the state-of-the-art methods,

it was also applied to the DIARETDB1 database [37].

Table 2. Obtained performance on DRIONS database.

Method	ACC%	CDD (pixel)	Overlap%
Carmona et al. [18]	96	5	-
Proposed method	100	9	76.5

In this experiment, the previous trained ANN using DRIONS dataset was used again. Since the training and test sets are really independent, the robustness of the proposed method can also be determined.

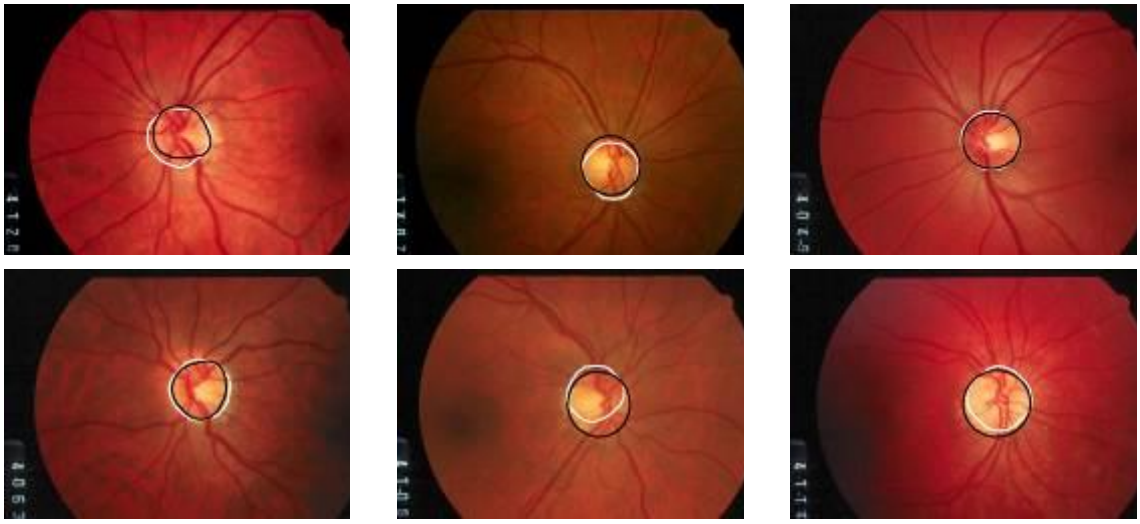

Figure 9. Results obtained for proposed method on DRIONS dataset images. Detected boundary of optic disc is shown by white curve, and ground truth is shown by black curve.

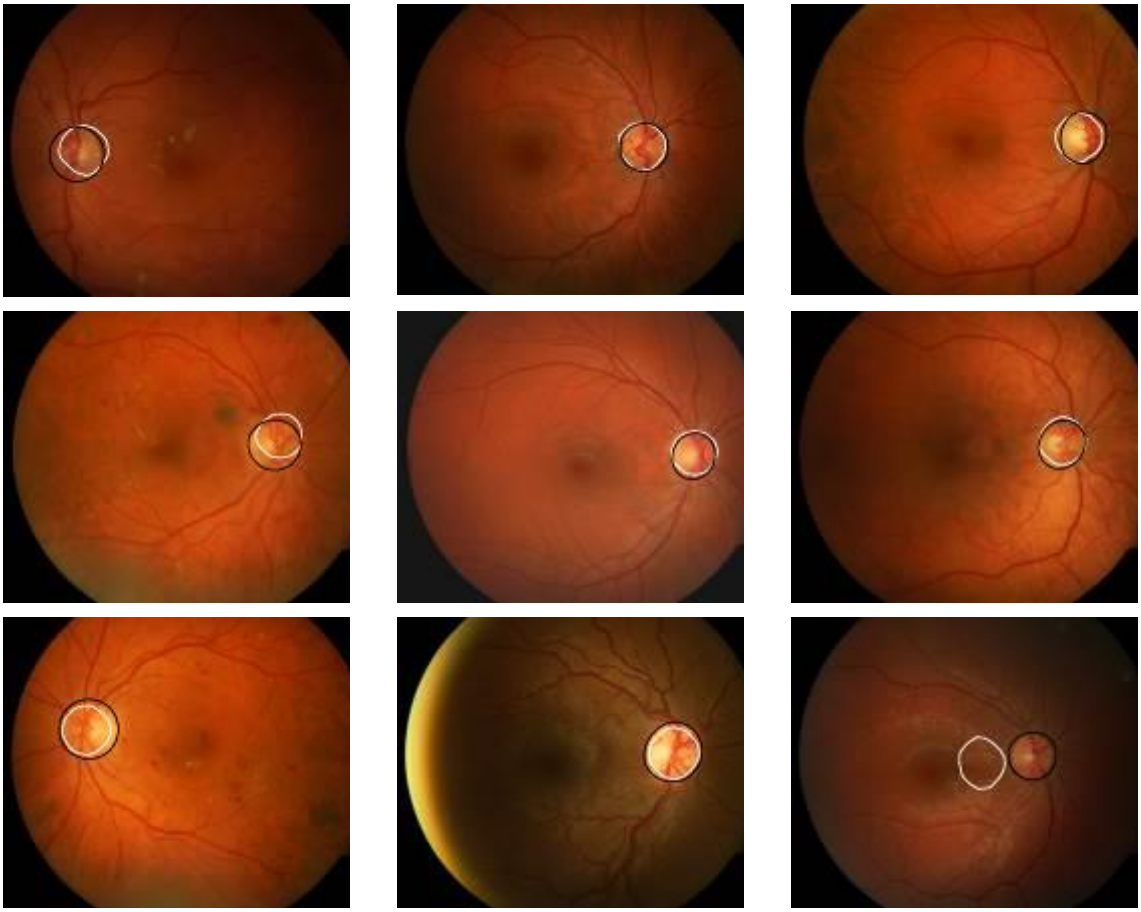

Figure 10. Results obtained for proposed method on DIARETDB1 dataset images. Detected boundary of optic disc is shown by white curve, and ground truth is shown by black curve.

Table 3. Obtained performance of all methods on DIARETDB1 database. Best values are bold.

Method	ACC%	CDD (pixel)	Overlap%	Sensitivity%	Predictive%
Walter et al. [16]	92.	15.5	37.2	65.6	93.9
Stapor et al. [17]	78.	6.0	34.1	84.9	80.3
Lupascu et al. [25]	86.	13.8	30.9	68.4	81.1
Sopharak et al. [27]	59.	16.3	29.7	46.0	95.9
Welfer et al. [28]	97.	4.9	44.5	92.5	87.6
Qureshi et al. [30]	94.	11.9	-	-	-
Proposed method	**95.**	**12.2**	**68.4**	**76.5**	**89.9**

Table 4. Obtained performance of all methods on DRIVE database. Best values are bold.

Method	ACC%	CDD (pixel)	Overlap%	Sensitivity%	Predictive%
Walter et al. [16]	77.5	12.39	30.03	49.88	86.53
Stapor et al. [17]	87.5	9.85	32.47	73.68	61.98
Youssif et al. [22]	100	17	-	-	-
Lupascu et al. [25]	95	8.05	40.35	77.68	88.14
Sopharak et al. [27]	95	20.94	17.98	21.04	93.34
Welfer et al. [28]	100	7.48	42.54	83.25	89.38
Qureshi et al. [30]	100	15.95	-	-	-
Hsiao et al. [31]	100	15	93	-	-
Ramakanth et al. [33]	100	-	-	-	-
Proposed method	**97.5**	**13.1**	**68.2**	**87.7**	**78.9**

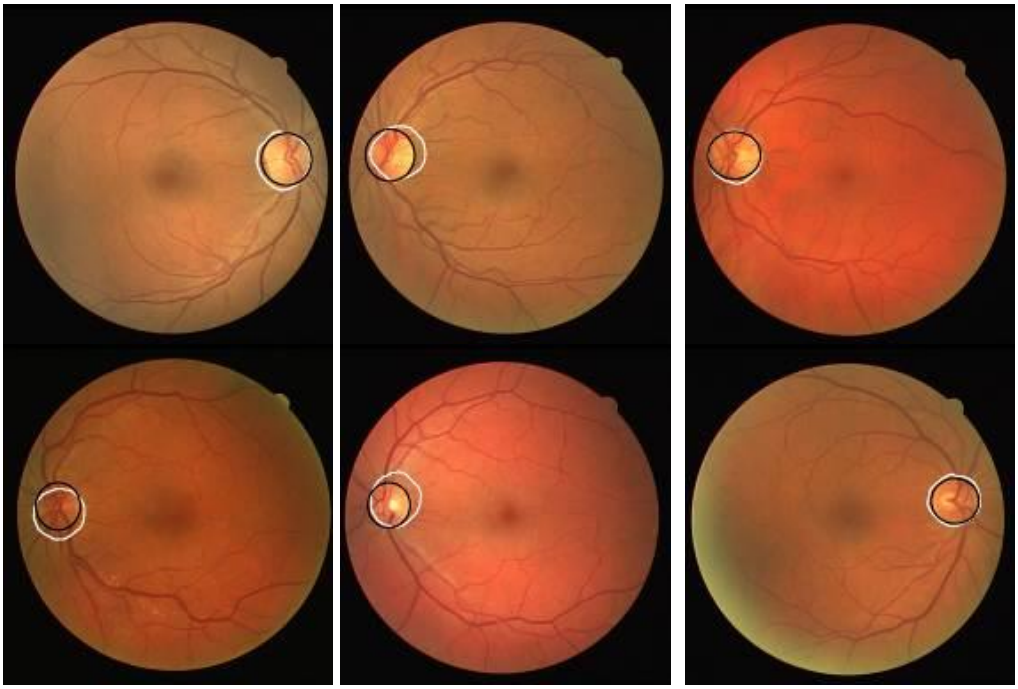

Figure 11. Results obtained for proposed method on some images of DRIVE dataset. Detected boundary of optic disc is shown by white curve, and corresponding ground truth is shown by black curve.

Table 5. Running times for different segmentation methods on DRIVE database. Best values are bold.

Method	Time	PC	Software
Walter et al. [16]	219.60s	Intel(R) Core (TM)2 Quad CPU 2.4 GHz, 4 GB RAM	MATLAB
Stapor et al. [17]	43.00s	Intel(R) Core (TM)2 Quad CPU 2.4 GHz, 4 GB RAM	MATLAB
Sopharak et al. [27]	14.92s	Intel(R) Core (TM)2 Quad CPU 2.4 GHz, 4 GB RAM	MATLAB
Welfer et al. [28]	22.66s	Intel(R) Core (TM)2 Quad CPU 2.4 GHz, 4 GB RAM	MATLAB
Proposed method	**13.24s**	Intel(R) Core (TM)2 Quad CPU 2.4 GHz, 4 GB RAM	MATLAB

For this purpose, the methods proposed by Walter et al. [16], Stapor et al. [17], Lupascu et al. [25], Sopharak et al. [27], Welfer et al. [28], and Qureshi et al. [30] were used for comparison. The results of other methods were obtained from their original papers or from Welfer et al. [28]. These results are summarized in table 3. In this table, for each evaluating parameter, the best value is bolded. The results obtained for the proposed method on some images of the DIARETDB1 database are also shown in figure 10.

From the results obtained, the overlap of the proposed method was much higher than the others (at least 22% greater), while its accuracy, sensitivity, and predictive values were high, and the mean distance between the center of detected optic disc and ground truth was about 12 pixels.

The proposed method was also compared on the DRIVE database [29] with some state-of-the-art methods. In this experiment, the methods proposed by Walter et al. [16], Stapor et al. [17], Youssif et al. [22], Lupascu et al. [25], Sopharak et al. [27] , Welfer et al. [28], Qureshi et al. [30], Hsiao et al. [31], and Ramakanth et al. [33] were used for comparison. The results of other methods were obtained from their original papers or from Welfer et al. [28]. These results are summarized in table 4. In this table, for each evaluating parameter, the best value is bolded. In this experiment, the previous trained ANN was used again. Since the training and test sets are really independent, the results obtained show the robustness of the proposed method. According to the results obtained, the sensitivity and overlap values for the proposed method were 87.7% and 68.2%, respectively, and higher than the others, while its accuracy, CDD, and predictive values were similar to the others. The results obtained for the proposed method on some images of the DRIVE database are also shown in figure 11.

Finally, the running time of the proposed method along with some state-of-the-art methods are given in table 5. The proposed method requires a low computational cost, and competes with the existing fast methods because we concentrated the feature extraction process only on the center line of the vessels. Without optimization of its MATLAB code, it will take about 13.2 seconds to process one image in the DRIVE database on a PC with a Intel(R) Core(TM)2 Quad CPU and 4.0 GB RAM. In real applications, the computation time can be significantly reduced by implementing the algorithm in C/C++ programming. In this way, our method can be seen as an interesting option to handle large image sets.

4. Conclusion

In this paper, we proposed an efficient algorithm for automatic optic disc detection and its border estimation. The proposed method is based upon estimating the similarity of the main retinal vessels into the optic disc vessels by employing the ANN along with efficient visual features of the optic discs vessels and background tissue. The center of detected inside the optic disc vessels was selected as the optic disc center, and a circle that surrounded these vessels was also selected as the initial border of the optic disc. The precise location of the optic disc boundary was adjusted by the radial analysis of the initial circle. The obtained average accuracy, overlap, sensitivity, and predictive values for optic disc segmentation on the DRIONS, DRIVE, and DIARETDB1 datasets were 97.7%, 70.6%, 80.3%, and 84.6%, respectively. The mean distance between the detected optic disc and ground truth was less than 12 pixels. The mean overlap value of the proposed method was at least 22% greater than the other state-of-the-art methods. Also the running time of the proposed method was better than the other state-of-the-art methods.

In the future works, to increase the performance of the proposed method, we can employ more reliable features, and also can employ feature learning-based techniques to this end. Also new edge detection methods [38] can be utilized to enhance results on noisy images. Finally employing other classifiers can be considered.

7. Acknowledgment

The author would like to thank Dr. Abdolhossein Fathi from Computer Engineering Department, Razi University, for his kind help and contribution in feature extraction and evaluation of results.

References

[1] Kose, C. & Ikibas, C. (2011). A personal identification system using retinal vasculature in retinal fundus images. Expert Sys. App., vol. 38, no. 11, pp. 13670-13681.

[2] Lathen, G., Jonasson, J. & Borga, M. (2010). Blood vessel segmentation using multi-scale quadrature filtering. Pattern Recognition Letters, vol. 31, pp. 762-767.

[3] Fathi, A. & Naghsh-Nilchi, A. R. (2013). Automatic Wavelet-Based Retinal Blood Vessels Segmentation and Vessel Diameter Estimation. Biomedical Signal Processing and Control, vol. 8, pp. 71– 80.

[4] Abdel-Ghafar, R. A., Morris, T., Ritchings, T., & Wood, I. (2004). Detection and characterisation of the optic disc in glaucoma and diabetic retinopathy,

presented at the Med. Image Understand. Anal. Conf., London, U.K., pp. 23-24.

[5] You, X., Peng, Q., Yuan, Y., Cheung, Y. & Lei, J. (2011). Segmentation of retinal blood vessels using the radial projection and semi-supervised approach. Pattern Recognition, vol. 44, no. 10-11, pp. 2314-2324.

[6] Manoj, S. & Muralidharan Sandeep, P. M. (2013). Neural Network Based Classifier for Retinal Blood Vessel Segmentation. International Journal of Recent Trends in Electrical & Electronics Engg, vol. 3, no. 1, pp. 44-53.

[7] Marin, D., Rábida, L., Aquino, A., Emilio, M., Arias, G. & Bravo, J.M. (2010). A New Supervised Method for Blood Vessel Segmentation in Retinal Images by Using Gray-Level and Moment Invariants-Based Features. IEEE Transactions on Medical Imaging. Vol. 30, no. 1, pp. 0278-0062.

[8] Vega, R., Guevara, E., Falcon, L. E., Sanchez, Ante, G. & Sossa, H. (2013). Blood Vessel Segmentation in Retinal Images Using Lattice Neural Networks. Advances in Artificial Intelligence and Its Applications, Vol. 8265, pp. 532-544.

[9] Chin, K. S., Trucco, E., Tan, L. & Wilson, P. J. (2013). Automatic fovea location in retinal images using anatomical priors and vessel density. Pattern Recognition Letters, vol. 34, pp. 1152-1158.

[10] Akram, M. U., Khalid, S., Tariq, A., Khan, S. A. & Azam, F. (2014). Detection and classification of retinal lesions for grading of diabetic retinopathy. Computers in Biology and Medicine, vol. 45, pp. 161-171.

[11] Abirami, P. K, Ganga, T. K., Regina, I. A. & Geetha, S. (2015). Neural Network based Classification and Detection of Glaucoma using Optic Disc and CUP Features. International Journal of Scientific Research Engineering & Technology, vol. 4, pp. 2321-0613.

[12] Vijayan, T. & Singh, A. (2015). Glaucoma Recognition and Segmentation Using Feed Forward Neural Network and Optical physics. International Journal of Advanced Research in Electrical, Electronics and Instrumentation Engineering, vol. 4, pp. 2320-3765.

[13] Wyawahare, M. V. & Patil, P. M. (2014). Performance Evaluation of Optic Disc Segmentation Algorithms in Retinal Fundus Images: an Empirical Investigation. International Journal of Advanced Science and Technology, vol. 69, pp. 19-32.

[14] Niemeijer, M., Abràmoff, M. D. & Ginneken, B.V. (2009). Fast detection of the optic disc and fovea in color fundus photographs. Med. Imag. Anal., vol. 13, pp. 859-870.

[15] Sinthanayothin, C., Boyce, D. J. F., Cook, H. L., & Williamson, T.H. (1999). Automated localization of the optic disc, fovea, and retinal blood vessels from digital colour fundus images. Ophthalmology, vol. 83, pp. 902-910.

[16] Walter, T., Klein, J. C., Massin, P. & Erginay, A. (2002). A contribution of image processing to the diagnosis of diabetic retinopathy - detection of exudates in color fundus images of the human retina. IEEE Trans. Med. Imag., vol. 21, no. 10, pp. 1236-1243.

[17] Stapor, K., Switonski, A., Chrastek, R. & Michelson, G. (2004). Segmentation of fundus eye images using methods of mathematical morphology for glaucoma diagnosis. Lecture Note. Comput. Scie., vol. 3039, pp.41-48.

[18] Carmona, E. J., Rincon, M., Garcıa-Feijoo, J. & De-la Casa, J.M.M. (2008). Identification of the optic nerve head with genetic algorithms. Artifi. Intel. Med., vol. 43, no. 3, pp. 243-259.

[19] Duanggate, C., Uyyanonvara, B., Makhanov, S. S., Barman, S. & Williamson, T. (2011). Parameter-free optic disc detection. Computerized Medical Imaging and Graphics, vol. 35, pp. 51-63.

[20] Hoover, A. & Goldbaum, M. (2003). Locating the optic nerve in a retinal image using the fuzzy convergence of the blood vessels. IEEE Trans. Med. Imag., vol. 22, no. 8, pp. 951-958.

[21] Welfer, D., Scharcanski, J., Kitamura, C. M., DalPizzol, M. M., Ludwig, L. W. B. & Marinho, D. R. (2010). Segmentation of the optic disc in color eye fundus images using an adaptive morphological approach. Comput. Bio. Med., vol. 40, pp.124-137.

[22] Youssif, A.A.H.A.R., Ghalwash, A. Z. & Ghoneim, A.A.S.A.R. (2008). Optic disc detection from normalized digital fundus images by means of a vessels' direction matched filter. IEEE Trans. Med. Imag., vol. 27, no. 1, pp. 11-18.

[23] Foracchia, M., Grisan, E. & Ruggeri, A. (2004). Detection of optic disc in retinal images by means of a geometrical model of vessel structure. IEEE Trans. Med. Imag., vol. 23, no. 10, p.p. 1189-1195.

[24] Morales, S., Naranjo, V., Angulo, J. & Alcaniz, M. (2013). Automatic Detection of Optic Disc Based on PCA and Mathematical Morphology. IEEE Transactions on Medical Imaging, vol. 32, no. 4, pp.786-796.

[25] Lupascu, C. A., Tegolo, D. & Rosa, L. D. (2008). Automated detection of optic disc location in retinal images. 21st IEEE Int. l Symp. Computer-Based Med. Sys., University of Jyvaskyla, Finland, pp.17-22.

[26] Pourreza-Shahri, R., Tavakoli, M. & Kehtarnavaz N. (2014). Computationally efficient optic nerve head detection in retinal fundus images. Biomedical Signal Processing and Control, vol. 11, pp. 63-73.

[27] Sopharak, A., Uyyanonvara, B., Barmanb, S. & Williamson, T. H. (2008). Automatic detection of diabetic retinopathy exudates from non-dilated retinal images using mathematical morphology methods. Comput. Med. Imag. Graph., vol. 32, pp. 720-727.

[28] Welfer, D., Scharcanski, J. & Marinho, D. R. (2013). A morphologic two-stage approach for automated optic disc detection in color eye fundus images. Pattern Recognition Letters, vol. 34, pp. 476-485.

[29] Tobin, K., Chaum, E., Govindasamy, V. & Karnowski, T. (2007). Detection of anatomic structures in human retinal imagery. IEEE Trans. Med. Imag., vol. 26, no. 12, pp. 1729-1739.

[30] Qureshi, R. J., Kovacs, L., Harangi, B., Nagy, B., Peto, T. & Hajdu, A. (2012). Combining algorithms for automatic detection of optic disc and macula in fundus images. Computer Vision and Image Understanding, vol. 116, pp. 138-145.

[31] Hsiao, H., Liu, C., Yu, C., Kuo, S. & Shen, S. (2012). A novel optic disc detection scheme on retinal images. Expert Systems with Applications, vol. 39, pp. 10600-10606.

[32] Mendonça, A. M., Sousa, A., Mendonça, L. & Campilho, A. (2013). Automatic localization of the optic disc by combining vascular and intensity information. Computerized Medical Imaging and Graphics, vol. 37, no. 5-6, pp. 409-417.

[33] Ramakanth, S. A. & Babu, R. V. (2014). Approximate Nearest Neighbour Field based Optic disc Detections. Computerized Medical Imaging and Graphics, vol. 38, pp. 49-56.

[34] Muramatsu, C., Nakagawa, T., Sawada, A., Hatanaka, Y., Hara, T., Yamamoto, T. & Fujita, H. (2011). Automated segmentation of optic disc region on retinal fundus photographs: Comparison of contour modeling and pixel classification methods. Computer methods and programs in biomedicine, vol. 101, pp. 23-32.

[35] Fathi, A., Naghsh-Nilchi, A. R. & Abdali-Mohammadi, F. (2013). Automatic vessel network features quantification using local vessel pattern operator. Computers in Biology and Medicine, vol. 43, pp. 587-593.

[36] DRIVE: Digital Retinal Images for Vessel Extraction. URL:http://www.isi.uu.nl/Research/ Databases /DRIVE/S.

[37] DIARETDB1: Kauppi, T., Kalesnykiene, V., Kamarainen, J.K., Lensu, L., Sorri, I., Raninen, A., Voutilainen, R., Uusitalo, H., alviainen, H. K¨ & Pietila, J., DIARETDB1 diabetic retinopathy database and evaluation protocol, Technical Report.

[38] Dorrani, Z. & Mahmoodi, M. S. (2016). Noisy images edge detection: Ant colony optimization algorithm. Journal of AI and Data Mining, Vol. 4, no. 1, pp. 77-83.

نشریه هوش مصنوعی و داده کاوی

تشخیص خودکار مرکز و حدود دیسک نوری در تصاویر رنگی شبکیه چشم

فردین ابدالی محمدی[1*] و امیر پورشمام[2]

[1] گروه کامپیوتر و فناوری اطلاعات، دانشکده فنی مهندسی، دانشگاه رازی، کرمانشاه، ایران.

[2] گروه ریاضی، دانشکده علوم پایه، دانشگاه رازی، کرمانشاه، ایران.

ارسال ۲۰۱۵/۱۱/۰۹؛ بازنگری ۲۰۱۶/۰۶/۱۸ پذیرش ۲۰۱۷/۰۳/۰۵

چکیده:

تشخیص دقیق نشانه‌های شبکیه مانند دیسک نوری گامی مهم در ابزارهای تشخیصی کامپیوتری می‌باشد. در این مقاله روشی کارا برای تشخیص خودکار مرکز دیسک نوری و حدود آن ارایه شده است. مرکز و قطر اولیه دیسک نوری با اعمال یک طبقه‌بند شبکه عصبی، تخمین زده می‌شود. در این روش ویژگی‌های تصویری رگ‌ها به همراه بافت زمینه آنها استفاده شده تا رگ‌های شبکیه به دو دسته تقسیم شوند: رگ‌های درون دیسک نوری و رگ‌های خارج دیسک نوری. برای نیل به این مقصود، مقدار میانگین شدت نور، انحراف معیار استاندارد کانال‌های RGB، میانگین پهنا و جهت رگ‌ها، تراکم رگ‌ها و نقاط تقاطع آنها در پنجره حول نقطه مرکزی رگ‌های اصلی به کار می‌روند. مرکز کشف شده رگ‌های اصلی که متعلق به ناحیه درون دیسک نوری هستند برای تخمین مرکز دیسک نوری به کار می‌روند و میانگین طول آنها در محورهای عمودی و افقی برای تخمین قطر دیسک نوری مورد استفاده قرار می‌گیرند. سپس قطر دقیق دیسک نوری با آنالیز شعاعی دایره تخمین زده اولیه به دست می‌آید. کارایی روش ارایه شده با استفاده از مجموعه داده‌های در دسترس DRIONS, DRIVE و DIARETDB1 ارزیابی شده و با آخرین روش‌های ارایه شده مقایسه شده است. روش ارایه شده میانگین همپوشانی بالاتری (۷۰/۶ درصد) با دقت یکسان برای محدوده دیسک (۹۷/۷ درصد) و فاصله تا مرکز (۱۲ پیکسل) نشان می‌دهد. حساسیت و p-value روش ارایه شده به ترتیب ۸۰/۳ و ۸۴/۶ درصد بوده است.

کلمات کلیدی: قطعه‌بندی تصاویر شبکیه، تشخیص مرکز دیسک نوری، تشخیص محدوده دیسک نوری.